# Supplementary Information:

## Tunable orbital Chern insulating states in crystalline Bernal-tetralayer graphene

**Contents**

1. Reproducibility for another device

2. Temperature dependence of magnetic hysteresis loops

3. Tight-binding model calculations

4. Electrical switching of Chern numbers for positive interlayer potential

5. Electrical switching of Chern numbers for negative interlayer potential

## 1. Reproducibility for another device

Fig. S1. presents the high-resolution maps of $R_{xx}$ and $R_{xy}$ measured under a small magnetic field of $B$ = 80 mT in device D2 and deivce D3. Consistent with Fig. 1e, f, in the main text, near the charge neutrality point (CNP) and for displacement fields $|D| \geq 0.15\,\mathrm{V/nm}$, $R_{xx}$ approached nearly zero, while the magnitude of $R_{xy}$ reached approximately $h/6e^2$.

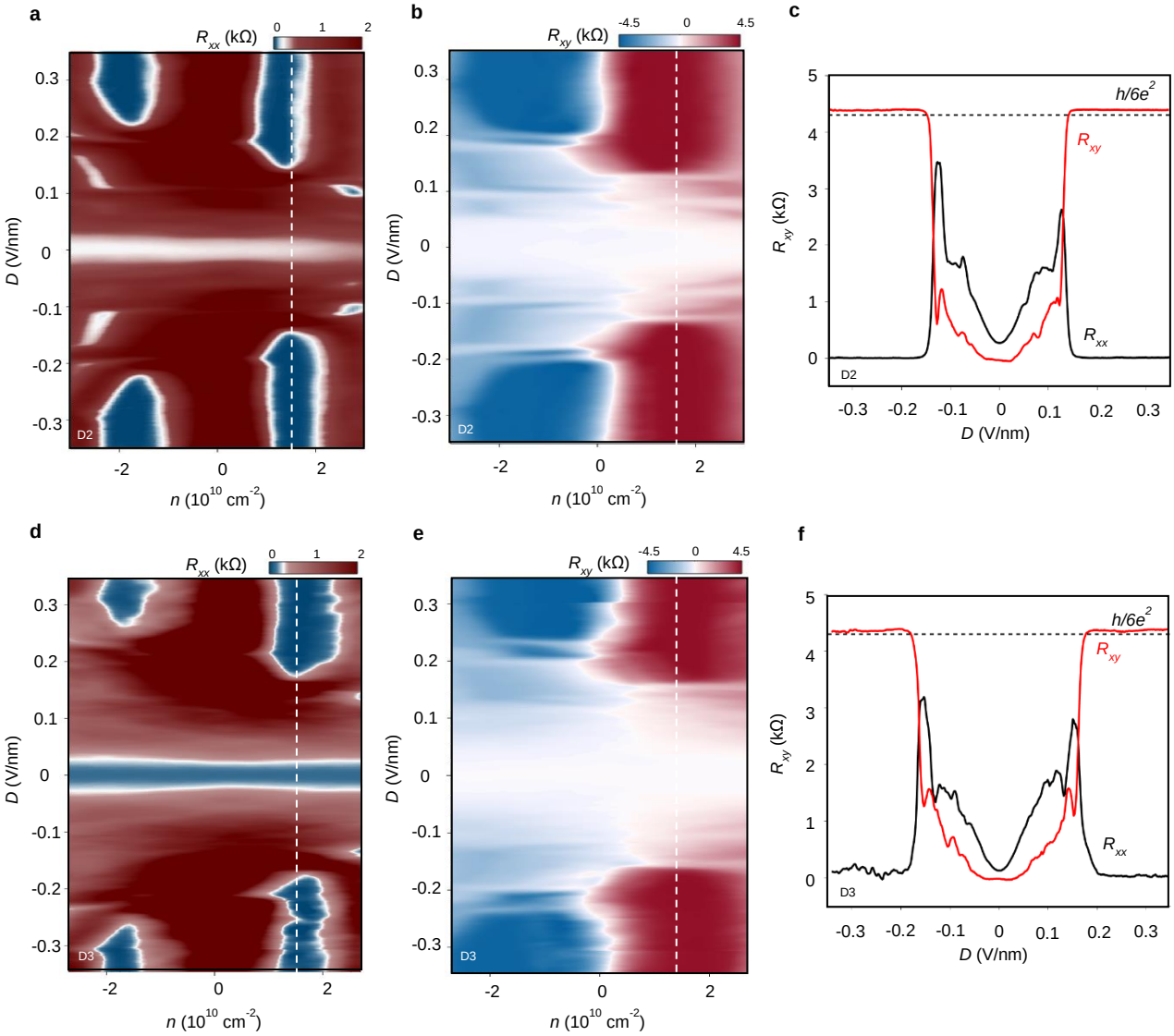


**Fig. S1. $n-D$ phase diagram at $B = 80$ mT of $R_{xx}$, $R_{xy}$ in device D2 and device D3. a, b,** Color plots of $R_{xx}$ (a) and $R_{xy}$ (b) as a function of $n$ and $D$ at $B = 80$ mT in device D2. **d, e,** Color plots of $R_{xx}$ (a) and $R_{xy}$ (b) as a function of $n$ and $D$ at $B = 80$ mT in device D3. Near at $|n| \sim 1.5 \times 10^{10}$ cm$^{-2}$ and $|D| > 0.15$ V/nm, $R_{xx}$ shows $\sim 0\,\Omega$, and $R_{xy}$ shows $\sim 4.3$ kΩ which corresponding Chern insulator with $C = 6$ in device D2 and device D3. **c, f,** Line cuts of $R_{xx}$(black) and $R_{xy}$(red) along the dashed line in (a), (b), (d), and (e).

This behavior is also evident in the line cuts of $R_{xx}$ and $R_{xy}$ as a function of displacement field at fixed carrier density of $n = 1.5 \times 10^{10}$ cm$^{-2}$. This phenomenon is absent from other nearby Landau level plateaus near the CNP, demonstrating that only the Chern number $C = 6$ uniquely manifests. These results highlight the remarkable reproducibility of the $C = 6$ Chern insulating states observed in Bernal stacked tetralayer graphene.

## 2. Temperature dependence of magnetic hysteresis loops

Fig. S2. Shows the temperature dependence of magnetic hysteresis loops of $R_{xy}$ in device D1. the hysteresis of $R_{xy}$ is measured at $n = 1.0 \times 10^{10}$ cm$^{-2}$, $D = 0.3$ V/nm, and temperature $T$ =10 mK to 15 K. The hysteresis loop disappears as the temperature increases to 15 K. However, $R_{xy}$ is quantized to $\sim \pm h/6e^2$ at $B = 80$ mT, $T < 5$ K. The phenomenon where the quantized Hall resistance disappears at low temperatures first, followed by the hysteric behavior persisting up to higher temperatures before vanishing, has been previously reported in various studies on the quantum anomalous Hall effect [1-2].

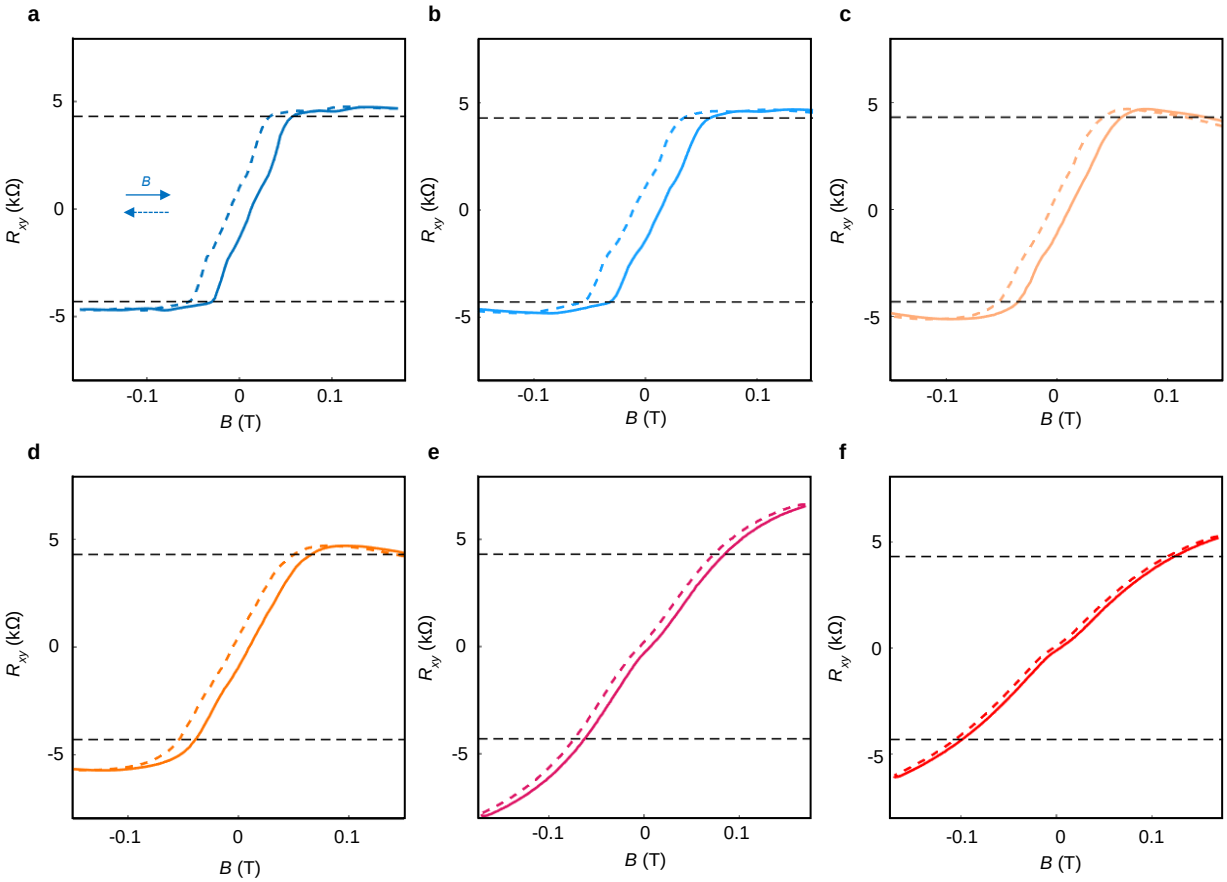


**Fig. S2. Temperature dependence of magnetic hysteresis loops in Device D1. a-f,** Magnetic hysteresis loops of $R_{xy}$ at $n = 1.0 \times 10^{10}$ cm$^{-2}$ and $D = 0.3$ V/nm at $T = 10$ mK(a), 1 K(b), 3 K(c), 5 K(d), 12 K(e), 15 K(f). Black dashed lines indicates quantized value of $\pm 4.3$ kΩ, which corresponds to a Chern number $C = \pm 6$.

## 3. Tight-binding model calculations

In this paper, we use the tight-binding model introduced in Ref. [3] and [4]. The Hamiltonian without considering the displacement field under basis $\psi = (A_1, B_1, A_2, B_2, A_3, B_3, A_4, B_4)^T$ can be expressed as:

$$H_0(\boldsymbol{k}) = \begin{pmatrix} H_{AB}^{12} & W \\ W^\dagger & H_{AB}^{34} \end{pmatrix},$$

where:

$$H_{AB}^{12} = H_{AB}^{34} = \begin{pmatrix} 0 & v_0\pi^\dagger & -v_4\pi^\dagger & v_3\pi \\ v_0\pi & \delta & \gamma_1 & -v_4\pi^\dagger \\ -v_4\pi & \gamma_1 & \delta & v_0\pi^\dagger \\ v_3\pi^\dagger & -v_4\pi & v_0\pi & 0 \end{pmatrix},$$

and

$$W = \begin{pmatrix} \gamma_2/2 & 0 & 0 & 0 \\ 0 & \gamma_5/2 & 0 & 0 \\ -\tilde{v}_4\pi & \Gamma_1 & \gamma_5/2 & 0 \\ \tilde{v}_3\pi^\dagger & -\tilde{v}_4\pi & 0 & \gamma_2/2 \end{pmatrix}.$$

In these matrices, $\pi = \zeta k_x + i\, k_y$ with $\zeta = \pm$ for $K$ and $K'$ valley, respectively. In addition, $v_i = \sqrt{3}a_0\gamma_i/2$, and $\tilde{v}_i = \sqrt{3}a_0\Gamma_i/2$, where $a_0 = 0.246$ nm is the lattice constant of graphene. The hopping parameters $\gamma_i$ and $\Gamma_i$ can be obtained from ab initio calculation as discussed in Ref. [3] and [5], and they are shown in Fig.1a in the main text.

The displacement field we considered in this paper is:

$$H_{12}^{AB} \to H_{12}^{AB} + \begin{pmatrix} \Delta & 0 & 0 & 0 \\ 0 & \Delta & 0 & 0 \\ 0 & 0 & \Delta/3 & 0 \\ 0 & 0 & 0 & \Delta/3 \end{pmatrix},$$

$$H_{34}^{AB} \to H_{34}^{AB} - \begin{pmatrix} \Delta & 0 & 0 & 0 \\ 0 & \Delta & 0 & 0 \\ 0 & 0 & \Delta/3 & 0 \\ 0 & 0 & 0 & \Delta/3 \end{pmatrix}.$$

It is worth mentioning that we consider the effect of the displacement field on the middle layers, as the bands near the Fermi surface are not solely contributed by atoms in the top and bottom

layers.

Using the tight-binding model, we can obtain the low-energy bands near the Fermi surface in each valley, as well as the Chern number for each band. At $K$ valley, the orbital components of the low energy bands are $(A_1, B_2, A_3, B_4)$. The results for $K$ valley under opposite interlayer potentials are presented in S3 and S4. The results for $K'$ valley can be obtained similarly. The orbital components of the low energy bands are also $(A_1, B_2, A_3, B_4)$; however, the Chern numbers for these four bands have opposite sign compared to those in the $K$ valley.

With the tight-binding model, we can get the low energy bands near the fermi surface in each valley and the Chern number for each band. The orbital components for each low-energy band can also be obtained. The result for $K$ valley is shown in Fig. S3.

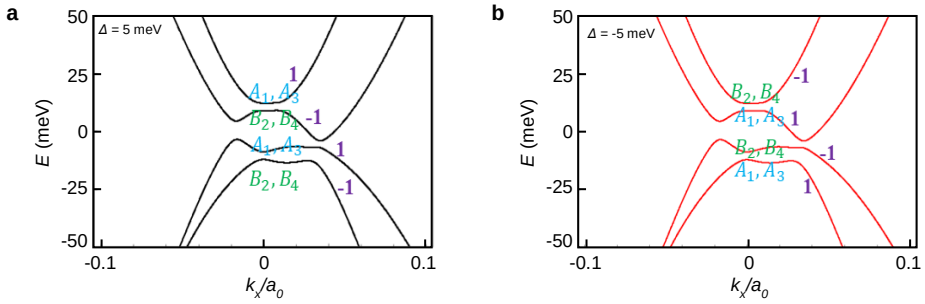


**Fig. S3. The low energy bands near the *K* points of BTG. a, b,** The low energy bands near the *K* points of BTG under positive (a) and negative (b) displacement field induced interlayer potentials are shown. The orbital components and the Chern number for each band are indicated in this figure.

## 4. Electrical switching of Chern numbers for positive interlayer potential

Next, we consider the LAFV order. The evolution of the band structure and Chern number in the two valleys explains the topological phase transition and the quantum anomalous Hall effect observed in experiments.

Under the basis $\psi\otimes(K,K')\otimes(\uparrow,\downarrow)$, the LAFV order parameter can be written as:

$$H_{LAFV}(\boldsymbol{k}) = (\sigma_0 \otimes \sigma_0 \otimes \sigma_z)\otimes(m_z\tau_z)\otimes s_0,$$

where $\sigma,\tau$ and $s$ denote the sublattice, valley, and spin degrees of freedom, respectively, and $m_z$ represents the amplitude of the LAFV order. $\sigma_0$ and $s_0$ are two-dimensional identity matrix, and $\sigma_i$, $\tau_i$, $s_i$ $(i = x,y,z)$ are Pauli matrices. Then we choose the amplitude of the LAFV to be $m_z = 6$ meV and calculate the band structure and Chern numbers under various interlayer potentials $\Delta$.

For *K* valley, the results are shown in Fig. S4a. The topological phase transition happens when the interlayer potential $\Delta = 4$ meV. For $K'$ valley, the band structure and Chern numbers can also be obtained. The result is shown in Fig. S4b. When the interlayer potential crosses $\Delta = 6$ meV and $\Delta = 15$ meV, the Chern number of each band changes. However, the total Chern number of the two valence bands in this valley remains zero. Combining these results in two valleys, we conclude that the appearance of the topological phase transition and the quantum anomalous Hall effect observed in experiment can be explained by the presence of the LAFV order in BTG. Additionally, the gap between conduction bands and valance bands $E_{gap}$ can also be obtained for all interlayer potentials.

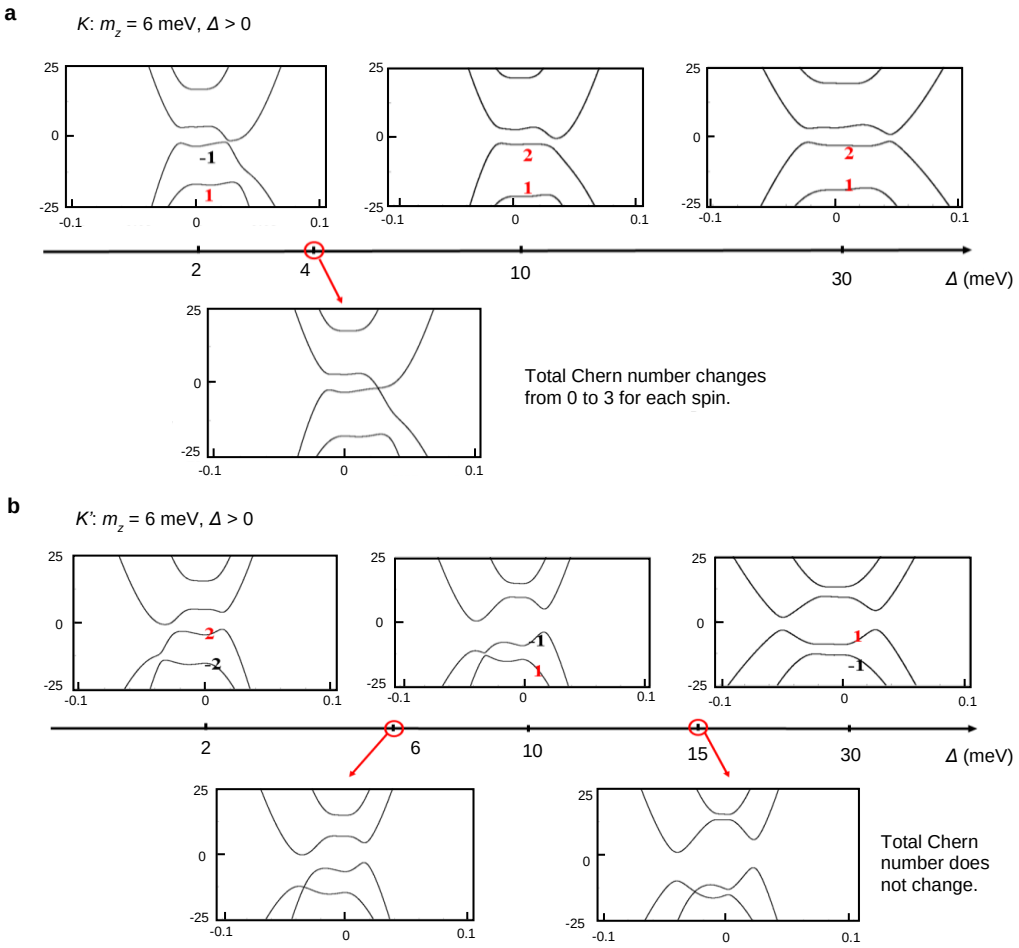


**Fig. S4. Tight binding model calculation and Electrical switching of Chern numbers at positive interlayer potential. a,** The band structure in $K$ valley of BTG under various positive interlayer potential $\Delta$ when considering the presence of LAFV order $m_z = 6$ meV. The topological phase transition happens when the interlayer potential is $\Delta = 4$ meV. **b,** The band structure in $K'$ valley of BTG under various positive interlayer potential $\Delta$ when considering the presence of LAFV order $m_z = 6$ meV. The total Chern number of the two valence bands remains zero as the interlayer potential increases.

89

90

## 5. Electrical switching of Chern numbers for negative interlayer potential

Then we calculate the band structure and Chern numbers under various negative interlayer potentials $\Delta$ for LAFV order $m_z = 6$ meV. For *K* valley, the results are shown in Fig. S5a. When the interlayer potential crosses $\Delta = -6$ meV and $\Delta = -15$ meV, the Chern number of each band changes. However, the total Chern number of the two valence bands in this valley remains zero. For *K'* valley, the results are shown in Fig. S5b. The topological phase transition happens when the interlayer potential $\Delta = -4$ meV. The total Chern number of the valence bands changes from 0 to 6. Therefore, we conclude that changing the sign of the displacement field does not change the sign of the Chern number in Chern insulating state.

However, when the LAFV order changes sign, i.e. $m_z = -6$ meV, we find that a topological phase transition occurs in $K'$ valley as the interlayer potential increases in positive direction ($\Delta > 0$). The Chern number for $K'$ valley changes from $0$ to $-6$, while the Chern number for $K$ valley remains $0$. Therefore, for $m_z = -6$ meV, an increasing interlayer potential induces a Chern insulating state with a total Chern number of $-6$. In addition, as the interlayer potential increases in negative direction ($\Delta < 0$), a topological phase transition occurs in $K$ valley, and the Chern number for $K$ valley changes from $0$ to $-6$, while the Chern number for $K'$ valley remains $0$, resulting in a total Chern number of $-6$.

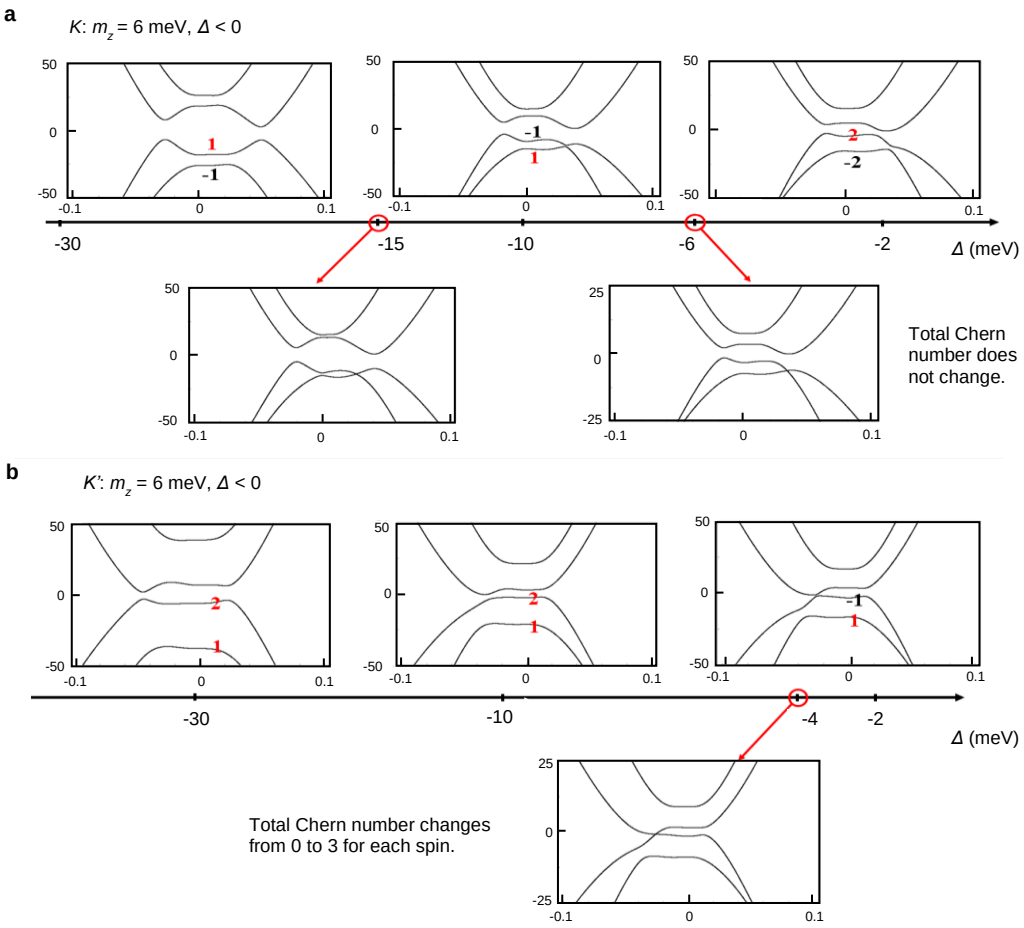


**Fig. S5. Tight binding model calculation and Electrical switching of Chern numbers at negative interlayer potential. a,** The band structure in $K$ valley of BTG under various negative interlayer potential $\Delta$ when considering the presence of LAFV order $m_z = 6$ meV. The total Chern number of the two valence bands remains zero as the interlayer potential decreases. **b,** The band structure in $K'$ valley of BTG under various negative interlayer potential $\Delta$ when considering the presence of LAFV order $m_z = 6$ meV. The topological phase transition occurs when the interlayer potential is $\Delta = -4$ meV.

## References


1. Li, T., Jiang, S., Shen, B. *et al.* Quantum anomalous Hall effect from intertwined moiré bands. *Nature* **600**, 641–646 (2021)
2. Han, T. *et al*. Large quantum anomalous Hall effect in spin-orbit proximitized rhombohedral graphene. *Science* **384**, 647–651 (2024)
3. Ghazaryan, A., Holder, T., Berg, E., Serbyn, M. Multilayer graphenes as a platform for interaction-driven physics and topological superconductivity. *Phys. Rev. B* **107**, 104502 (2023)
4. Aoki, M., Amawashi, H. Dependence of band structures on stacking and field in layered graphene. *Solid State Commun.* **142**, 123–127 (2007)
5. Chen, H., Arora, A., Song, J. C., Loh, K. P. Gate-tunable anomalous Hall effect in Bernal tetralayer graphene. *Nat. Commun.* **14**(1), 7925 (2023)